The Astrophysical Journal Letters, 709:L16–L20, 2010 January 20 doi:10.1088/2041-8205/709/1/L16

$z \sim 7$ GALAXIES IN THE HUDF: FIRST EPOCH WFC3/IR RESULTS*

P. A. Oesch[1], R. J. Bouwens[2,3], G. D. Illingworth[2], C. M. Carollo[1], M. Franx[3], I. Labbé[4,8], D. Magee[2], M. Stiavelli[5], M. Trenti[6], and P. G. van Dokkum[7]
[1] Institute for Astronomy, ETH Zurich, 8092 Zurich, Switzerland; poesch@phys.ethz.ch
[2] UCO/Lick Observatory, University of California, Santa Cruz, CA 95064, USA
[3] Leiden Observatory, Leiden University, NL-2300 RA Leiden, The Netherlands
[4] Carnegie Observatories, Pasadena, CA 91101, USA
[5] Space Telescope Science Institute, Baltimore, MD 21218, USA
[6] University of Colorado, Center for Astrophysics and Space Astronomy, 389-UCB, Boulder, CO 80309, USA
[7] Department of Astronomy, Yale University, New Haven, CT 06520, USA
Received 2009 September 10; accepted 2009 December 4; published 2009 December 29

ABSTRACT

We present a sample of 16 robust $z \sim 7$ z_{850}-drop galaxies detected by the newly installed Wide Field Camera 3 (WFC3)/IR on the *Hubble Space Telescope*. Our analysis is based on the first epoch data of the HUDF09 program covering the Hubble Ultra Deep Field with 60 orbits of Y_{105}, J_{125}, and H_{160} observations. These remarkable data cover 4.7 arcmin^2 and are the deepest near infrared images ever taken, reaching to ∼29 mag AB (5σ). The 16 $z \sim 6.5$–7.5 galaxies have been identified based on the Lyman Break technique utilizing ($z_{850} - Y_{105}$) versus ($Y_{105} - J_{125}$) colors. They have magnitudes $J_{125} = 26.0$–29.0 (AB), an average apparent half-light radius of ∼0.16 arcsec ($\lesssim$1 kpc), and show very blue colors (some even $\beta \lesssim -2.5$), in particular at low luminosities. The WFC3/IR data confirm previous Near Infrared Camera and Multi-Object Spectrometer detections indicating that the dropout selection at $z \sim 7$ is very reliable. Our data allow a first determination of the faint-end slope of the $z \sim 7$ luminosity function, reaching down to $M_{\rm UV} \sim -18$, a full magnitude fainter than previous measurements. When fixing $\phi_* = 1.4 \times 10^{-3}$ Mpc^{-3} mag^{-1} to the value previously measured at $z \sim 6$, we find a best-fit value of $\alpha = -1.77 \pm 0.20$, with a characteristic luminosity of $M_* = -19.91 \pm 0.09$. This steep slope is similar to what is seen at $z \sim$ 2–6 and indicates that low-luminosity galaxies could potentially provide adequate flux to reionize the universe. The remarkable depth and resolution of these new images provide insights into the coming power of the *James Webb Space Telescope*.

Key words: galaxies: evolution – galaxies: high-redshift – galaxies: luminosity function, mass function

1. INTRODUCTION

While great progress has been made in the study of galaxies up to $z \sim 6$, even after more than a decade of Lyman break galaxy (LBG) surveys, the samples of UV-selected candidate $z \gtrsim 7$ galaxies are still very modest (e.g., Bouwens et al. 2004b, 2008; Yan & Windhorst 2004; Bradley et al. 2008; Richard et al. 2008; Oesch et al. 2009a; Zheng et al. 2009; Ouchi et al. 2009; Castellano et al. 2009). Due to their small number, the $z \gtrsim 7$ luminosity function (LF), and in particular its faint-end slope, is still very uncertain. An accurate measurement of this is of fundamental importance, however, not only for the early stages of galaxy formation, but also for the understanding of the epoch of reionization and the role of galaxies therein.

For sources of such early cosmic times the intergalactic medium absorbs most of the light blueward of Lyα, which is redshifted into the near-infrared (NIR), where the sensitivities and fields of view of the detectors have lagged behind the optical CCD cameras. Extremely deep NIR imaging is needed to detect these galaxies. Moreover, due to limited spatial resolution of earlier IR cameras, it has not been possible so far to measure other basic quantities of $z \sim 7$ galaxies such as sizes.

With the installation of the Wide Field Camera 3 (WFC3) in Service Mission 4 of the *Hubble Space Telescope* (*HST*) a new era of high-redshift galaxy surveys has begun. With its large area, high sensitivity, and small pixel size, it allows us to probe faint objects much more efficiently than *HST*'s previous NIR camera Near Infrared Camera and Multi-Object Spectrometer (NICMOS). Additionally, WFC3's improved filter set over NICMOS helps us to exclude contaminating interloper objects and to estimate more precise photometric redshifts for these sources. Furthermore, it allows for the first time the detection of galaxies at $z \sim 8$, which we report on in an accompanying paper (Bouwens et al. 2009b).

In this Letter, we present early results on our search for $z \sim 7$ galaxies from the first epoch data of the HUDF09 survey. In Section 2, we describe the data, the $z \sim 7$ candidate selection and its efficiency. In Section 3, we present new constraints on the LBG LF at $z \sim 7$. We adopt $\Omega_M = 0.3$, $\Omega_\Lambda = 0.7$, $H_0 = 70$ km s^{-1} Mpc^{-1}, i.e., $h = 0.7$. Magnitudes are given in the AB system (Oke & Gunn 1983).

2. OBSERVATIONS AND SOURCE SELECTION

2.1. The HUDF09: First Epoch Data

The HUDF09 program will cover the Hubble Ultra Deep Field (HUDF; Beckwith et al. 2006) with a total of 96 orbits of WFC3/IR observations in three filters. These are H_{160} (F160W), J_{125} (F125W), and Y_{105} (F105W). The first epoch data available now have been taken between 2009 August 26 and 2009 September 6 and consist of 62 orbits reaching a uniform point-source depth in all filters of 28.6–28.7 (5σ AB, in 0.″25 radius apertures). The data set covers an area of 4.7 arcmin^2 and has a point-spread function (PSF) FWHM of ∼0.″16. It already allows us to generate the deepest NIR images ever seen.

* Based on data obtained with the *Hubble Space Telescope* operated by AURA, Inc. for NASA under contract NAS5-26555.
[8] Hubble Fellow.

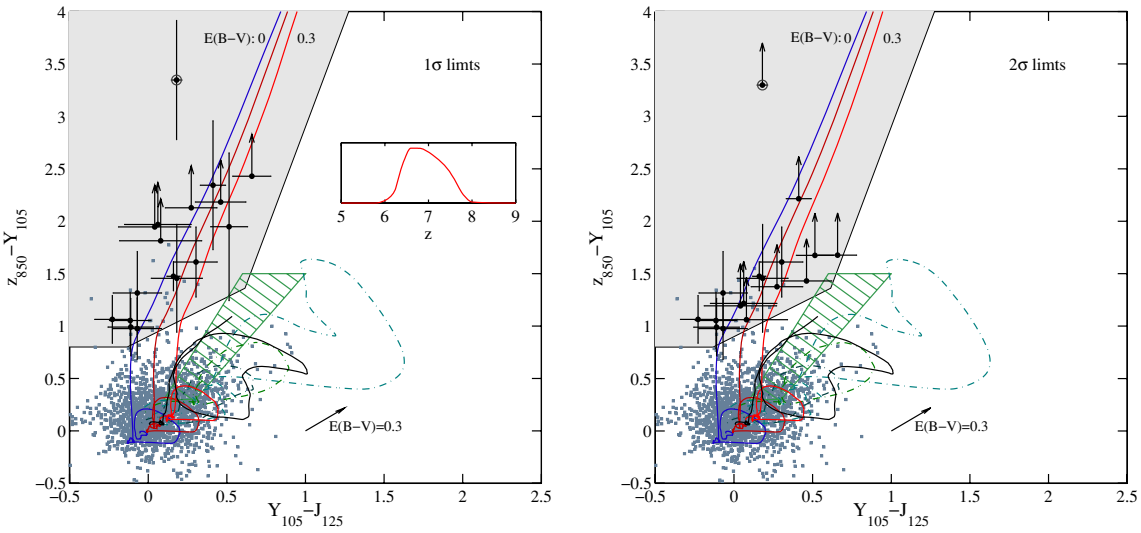

Figure 1. Color–color diagram used for the selection of $z \sim 7$ z_{850} dropout galaxies. Left: 1σ limits are used when measuring colors, right: the same with 2σ limits. The gray points indicate all galaxies in the catalog and black dots are 17 candidates with no detections in the optical. As mentioned in the text, the reddest of these is very likely to be a SN (marked with a dark gray circle) and is excluded in our further analysis. Tracks of star-forming galaxies, obtained with Bruzual & Charlot (2003) models, are shown with solid lines in blue-to-red colors corresponding to dust obscurations of $E(B-V) = 0,\ 0.15,\ 0.3$. Low-redshift galaxy tracks up to redshift $z = 5$ are derived from the galaxy templates of Coleman et al. (1980) and are shown as dash-dotted lines. Additionally, we plot the track of a simple stellar population with an age of 500 Myr as a solid black line. The green hatched region covers the locus of M, L, and T dwarf stars derived by convolving observed spectra from Burgasser et al. (2004) as well as theoretical template SEDs of Burrows et al. (2006) with the WFC3 filter curves. The black arrow indicates the reddening vector with $E(B-V) = 0.3$ at redshift 1.5 and with a Calzetti et al. (2000) reddening curve. Low-redshift galaxies in our selection window are typically described by very young SEDs with strong nebular line and continuum emission. These galaxies are, however, well detected in the optical data, and they all lie within 1σ of our selection window. The inset in the left panel shows the estimated redshift distribution expected for our color selection.

The images have been reduced using standard techniques. A super median image was subtracted from all frames before coadding them to an image of 0.″06 pixel scale registered to the NICMOS HUDF images (Thompson et al. 2005, including the deep UDF05 pointing; see Oesch et al. 2007, 2009a) using our own modified version of `multidrizzle` (Koekemoer et al. 2002). Only ground-based calibration data for WFC3 were available at the time of this analysis. Therefore, image distortion maps have been derived by us based on relatively bright sources in the Advanced Camera for Surveys (ACS) HUDF.

We have found that persistence in severely saturated pixels from prior observations can have a noticeable effect on subsequent observations, even hours after the saturation has taken place. The affected pixels have been masked out before further processing. However, two orbits of Y_{105} data were completely excluded.

We have checked the photometric zero points based on spectral energy distribution (SED) fitting to the well-calibrated and PSF-matched ACS and NICMOS data, which resulted in values very similar (<0.05 mag) to the space based zero points derived by STScI. We therefore opted to use the official values in our subsequent analysis.

2.2. z_{850}-dropout Candidate Selection

The summed J_{125}+Y_{105} image is used to detect galaxies with the SExtractor program (Bertin & Arnouts 1996) and to measure their colors in isophotal apertures after the optical images have been PSF-matched to the WFC3/IR exposures. Total magnitudes are measured in 2.5 Kron (AUTO) apertures and small corrections of 0.1 mag have been applied to account for flux loss in the wings of the PSF.

Only sources with signal-to-noise ratio (S/N) larger than 5 within 0.″25 radius apertures in both J_{125}- and Y_{105}-images are considered. We have ensured that our weight maps correctly reproduce the appropriate noise properties in these apertures and measured fluxes $< 1\sigma$ were replaced by a $1-\sigma$ upper limit.[9]

Galaxies are selected from the SExtractor catalog based on the Lyman Break technique (e.g., Steidel et al. 1996; Giavalisco et al. 2004; Bouwens et al. 2007) requiring

$$(z_{850} - Y_{105}) > 0.8$$
$$(z_{850} - Y_{105}) > 0.9 + 0.75(Y_{105} - J_{125})$$
$$(z_{850} - Y_{105}) > -1.1 + 4(Y_{105} - J_{125})$$
$$\mathrm{S/N}(J_{125}) > 5 \wedge \mathrm{S/N}(Y_{105}) > 5$$
$$\mathrm{S/N}(V_{606}) < 2 \wedge \mathrm{S/N}(i_{775}) < 2.$$

These criteria select galaxies from $z \sim 6.4$–7.3 with a median redshift of $\langle z \rangle = 6.8$; see the inset of Figure 1.

After rejecting spurious sources such as diffraction spikes of stars and one probable supernova, we find 16 $z \sim 7$ candidates between $J_{125} = 26.0$ and 29.0 mag. Their properties are listed in Table 1, and an image of all candidates is shown in Figure 2. As can be seen from Table 1, the $J_{125} - H_{160}$ colors of these sources are extremely blue, in particular toward faint J_{125} magnitudes, which results in UV-continuum slopes as steep as $\beta \lesssim -2.5$. This could imply that these sources are dominated by very metal-poor stars with little to no dust extinction, or alternatively exhibit initial mass functions skewed toward massive stars. All these possibilities would have strong implications for the ionizing flux produced by these galaxies, which may be larger than what is assumed in current calculations of reionization (see Bouwens et al. 2009d).

It is reassuring that all $z \sim 7$ galaxy candidates, which have been identified in previous work, are confirmed to be secure high-redshift candidates (see Table 1). We show in Figure 3

[9] We also checked that the use of $2-\sigma$ limits does not change our results significantly. In Figure 1, we show the photometry using both limits.

Table 1
Photometry (AB mag) of the $z \sim 7$ z_{850}-dropout Sources[a]

ID	α	δ	J_{125}	$z_{850} - Y_{105}$	$Y_{105} - J_{125}$	$J_{125} - H_{160}$	S/N$_{J125}$	Reference
UDFz-42566566	03:32:42.56	−27:46:56.6	25.95 ± 0.04	1.48 ± 0.14	0.16 ± 0.04	−0.08 ± 0.04	25.8	1, 2, 3, 4, 5, 6
UDFz-44716442	03:32:44.71	−27:46:44.2	26.90 ± 0.10	>2.43	0.66 ± 0.12	−0.25 ± 0.09	17.2	×
UDFz-38807073	03:32:38.80	−27:47:07.3	26.90 ± 0.06	2.34 ± 0.61	0.41 ± 0.08	0.14 ± 0.06	26.2	1, 2, 4, 5, 6, 7
UDFz-39557176	03:32:39.55	−27:47:17.6	27.19 ± 0.08	1.95 ± 0.70	0.51 ± 0.12	0.04 ± 0.09	14.8	2, 5
UDFz-42577314	03:32:42.57	−27:47:31.4	27.22 ± 0.20	1.61 ± 0.33	0.30 ± 0.14	−0.16 ± 0.12	11.1	2, 5, 6
UDFz-39586565	03:32:39.58	−27:46:56.5	27.74 ± 0.18	0.99 ± 0.27	−0.11 ± 0.15	−0.32 ± 0.18	9.3	–
UDFz-37228061	03:32:37.22	−27:48:06.1	27.76 ± 0.14	>2.18	0.46 ± 0.16	−0.08 ± 0.13	11.3	–
UDFz-43146285	03:32:43.14	−27:46:28.5	27.81 ± 0.20	>2.13	0.27 ± 0.16	0.04 ± 0.14	10.3	×
UDFz-36777536	03:32:36.77	−27:47:53.6	27.83 ± 0.16	1.06 ± 0.23	−0.23 ± 0.11	−0.13 ± 0.13	13.5	–
UDFz-37446513	03:32:37.44	−27:46:51.3	27.86 ± 0.16	1.05 ± 0.27	−0.11 ± 0.13	−0.06 ± 0.14	11.4	–
UDFz-40566437	03:32:40.56	−27:46:43.7	27.97 ± 0.17	1.32 ± 0.40	−0.07 ± 0.15	−0.43 ± 0.20	7.7	–
UDFz-41057156	03:32:41.05	−27:47:15.6	28.08 ± 0.16	1.46 ± 0.51	0.18 ± 0.16	−0.16 ± 0.16	10.7	–
UDFz-36387163	03:32:36.38	−27:47:16.3	28.27 ± 0.18	0.98 ± 0.29	−0.07 ± 0.15	−0.12 ± 0.17	9.8	–
UDFz-37807405	03:32:37.80	−27:47:40.5	28.36 ± 0.16	>1.97	0.06 ± 0.21	−0.27 ± 0.24	6.8	–
UDFz-39736214	03:32:39.73	−27:46:21.4	28.56 ± 0.20	>1.95	0.04 ± 0.23	−0.41 ± 0.28	5.9	–
UDFz-38537519	03:32:38.53	−27:47:51.9	28.96 ± 0.24	>1.81	0.08 ± 0.26	−0.62 ± 0.36	5.8	–
UDF-34537360[b]	03:32:34.53	−27:47:36.0	25.96 ± 0.03	3.35 ± 0.57	0.18 ± 0.03	0.21 ± 0.03	50.0	

Notes.
[a] The J_{125} photometry was derived from elliptical apertures of 2.5 Kron radii, and has been corrected to total magnitudes by 0.1 mag offsets, while colors were measured in isophotal apertures. Limits correspond to 1σ.
[b] This object is most likely a supernova, as it is very bright and has a stellar profile. It should have been securely detected in the previous NICMOS images, and we therefore exclude it from any further analysis.
References. (1) Bouwens & Illingworth 2006; (2) Bouwens et al. 2004b; (3) Yan & Windhorst 2004; (4) Coe et al. 2006; (5) Labbé et al. 2006; (6) Bouwens et al. 2008; and (7) Oesch et al. 2009a: (×) not covered by NICMOS data and (−) no previous detection.

a comparison of the NICMOS observations with the WFC3 data for the brightest candidates which were covered by both instruments in order to visualize the enormous improvement in data quality provided by WFC3/IR. The new data allow us to probe much fainter limits. While in previous studies only two galaxies were identified beyond a magnitude of 27.5, of which one is only marginally detected (Bouwens et al. 2008; Oesch et al. 2009a), the current WFC3 sample includes 11 such faint objects, resulting in much better constraints on the LF at $z \sim 7$.

2.3. Sources of Sample Contamination

Previous $z \sim 7$ selections have suffered from several possible sources of contamination, such as (1) spurious detections, (2) cool dwarf stars, (3) intermediate redshift galaxies with red optical–NIR colors, (4) lower redshift sources which scatter into the selection due to photometric errors, and (5) high-redshift supernovae. Our HUDF09 WFC3/IR observations are much less affected by these problems as we briefly discuss below.

(1) The sources presented in this Letter are virtually all $>5\sigma$ detections in three bands, which have been obtained with different dither positions, and the noise properties of WFC3/IR are much better behaved than in NICMOS data. Thus we rule out that any of our source is a spurious detection or is caused by an image artifact.[10]

(2) As can be seen in Figure 1, dwarf stars occupy a different locus in the $z_{850} - Y_{105}$ versus $Y_{105} - J_{125}$ diagram than high-redshift galaxies. The J_{125} band probes short enough wavelengths that it is not dominated by the strong absorption bands of dwarf star SEDs. Therefore, it is very unlikely that any such source contaminates our sample.[11]

(3) and *(4)* The $z \sim 7$ galaxy candidates are covered with three bands, all showing colors bluer than expected for possible low-redshift contaminants. Based on simulations in which we add photometric errors to galaxies in the magnitude range $J_{125} = 24$–25.9, simulating the photometry of galaxies down to $J_{125} = 29$, we find a negligible contamination fraction by lower redshift interlopers (<0.3%). These simulations are based on the assumption that bright galaxies follow the same SED distribution as at fainter magnitudes, which is not likely to be true. In fact, the fainter population shows slightly bluer $z - Y$ colors, which would result in an even smaller contamination rate in the observations than in our simulations. However, the only galaxies with intrinsic SEDs of sufficiently blue NIR colors and which may remain undetected in the optical are very young ($<10^7$ yr) $z \sim 1.5$ galaxies with strong emission lines. Given their peculiar SEDs and their extreme faintness being at $z \sim 1.5$, such galaxies are not expected to be very common, even though their exact number density is unknown. We are thus confident that our selection is essentially free from low-redshift contaminants.

(5) Since our WFC3/IR observations are taken much later than the already existing optical data, supernovae are a potential source of contamination of our sample. Following the calculation in Bouwens et al. (2008), however, only 0.012 sources are expected to be found per arcmin^2, which results in ∼0.06 expected supernovae. Fortunately, at the bright end, such sources can be eliminated by comparison to the existing NICMOS images. Indeed, we find one such source, which shows a stellar profile and, with $J_{125} = 26.0$ mag, should have been securely detected in the previous NICMOS images of the HUDF (see Table 1). We exclude this source from our subsequent analysis, but list it here because of its potential interest.

3. THE $z \sim 7$ LBG LUMINOSITY FUNCTION

As in Oesch et al. (2007, 2009a), completeness, C, and magnitude-dependent redshift selection probabilities, S, for

[10] It is furthermore reassuring that after submission of this manuscript McLure et al. (2009b) and Bunker et al. (2009) have independently identified a very similar set of $z \sim 7$ galaxy candidates from the same data set used in this work.
[11] Note that the *HST* $z_{850} - Y_{105}$ colors are bluer than $(z - Y)_{AB}$ colors reported for T dwarfs from ground-based measurements (e.g., Pinfield et al. 2008) due to the wider Y_{105}.

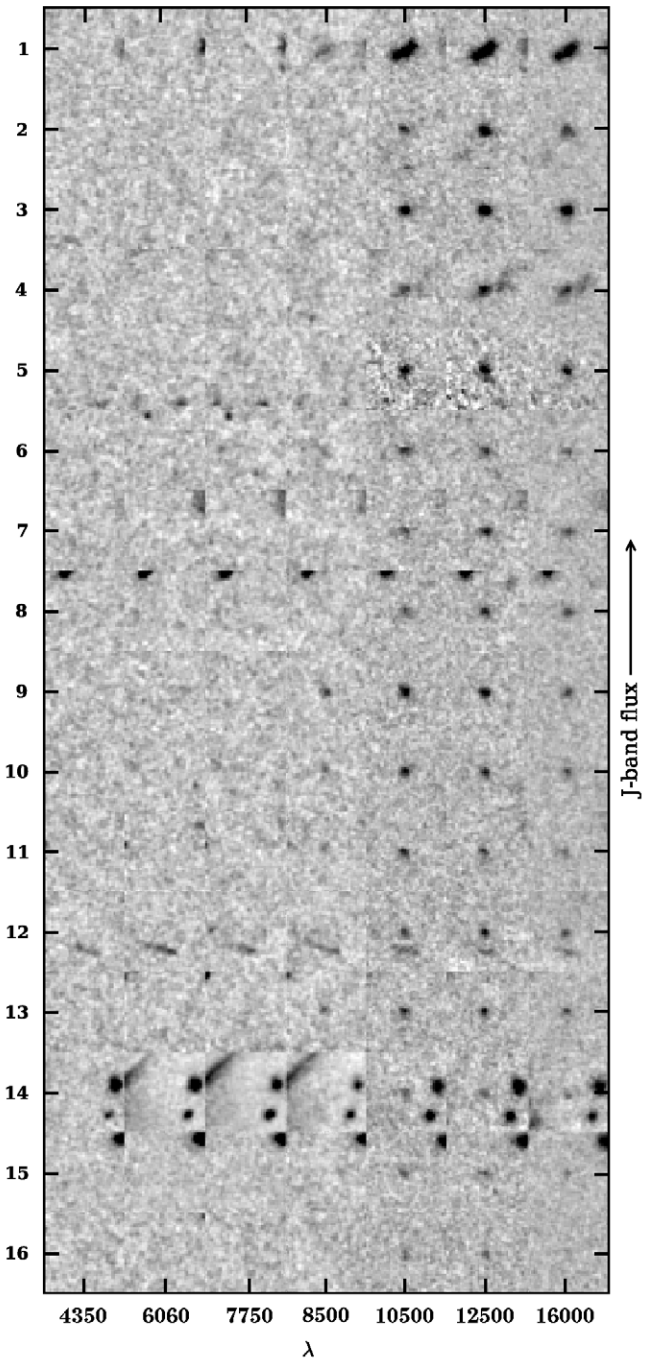

Figure 2. All $z \sim 7$ galaxy candidates in B_{435}, V_{606}, i_{775}, z_{850}, Y_{105}, J_{125}, and H_{160} (from left to right), ranked by their J_{125}-flux (see also Table 1). The sizes of the images are $2\farcs2 \times 2\farcs2$.

our sample are derived from simulations in which we add artificial galaxies into the real images and rerun our detection and selection procedure. The input SED distribution for these simulations is chosen to be slightly steeper than the measured slopes for $z \sim 6$ galaxies ($\beta = -2.2$; Stanway et al. 2005; Bouwens et al. 2009c) to account for the very blue colors seen in our sample ($\beta \sim -2.5$, see also Bouwens et al. 2009d), and a log-normal size distribution with a size scaling of $(1+z)^{-1}$ (Ferguson et al. 2004; Bouwens et al. 2004a; Oesch et al. 2009b) is assumed.

The LF brightens significantly from $z \sim 6$ to $z \sim 4$ (e.g., McLure et al. 2009a; Bouwens et al. 2007; Bouwens

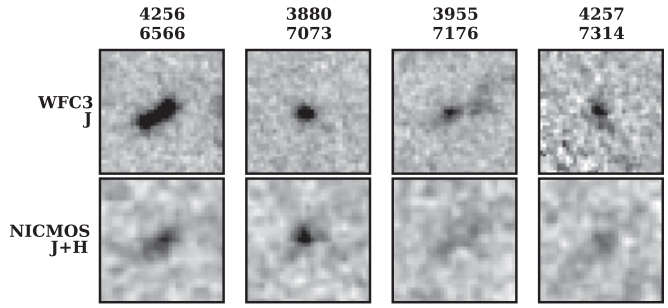

Figure 3. Comparison of WFC3 J_{125} (top) and NICMOS F110W+F160W (bottom; Thompson et al. 2005) images for the brightest z_{850}-dropout galaxies, showing the improvement in data quality. Only galaxies covered with both instruments are shown.

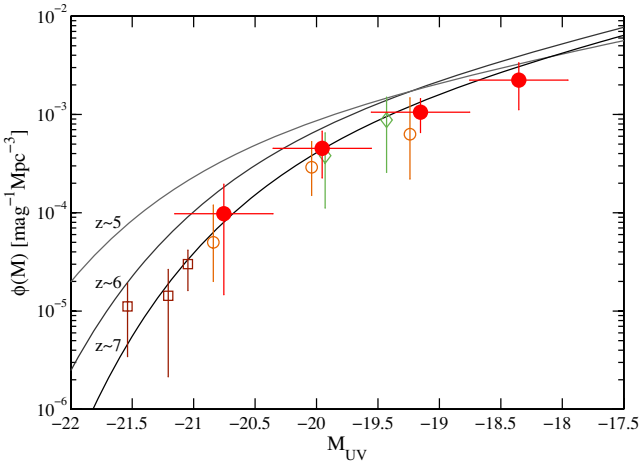

Figure 4. $z \sim 7$ LBG LF derived from the WFC3 candidates (filled red circles). The black solid line corresponds to our best-fit LF with $\alpha = -1.77$, $\phi_* = 1.4 \times 10^{-3}$ Mpc^{-3}mag^{-1}, and $M_* = -19.91$. This value of the faint-end slope is consistent with no evolution since $z \sim 2$ (e.g., Bouwens et al. 2007; Oesch et al. 2007; Reddy et al. 2009). Data points from previous estimates are shown as open symbols; orange circles: Bouwens et al. (2008), green diamonds: Oesch et al. (2009a), dark red squares: Ouchi et al. (2009). The latter ones have been used in our fit to constrain the bright end of the LF. The remaining lines show the LF at $z \sim 5$ (light gray solid line: Oesch et al. 2007), and $z \sim 6$ (dark gray solid line: Bouwens et al. 2007). Note that the $z \sim 7$ points of Bouwens et al. (2008) and Oesch et al. (2009a) are partially based on NICMOS data from the HUDF and are thus not independent from our measurements.

& Illingworth 2006; Oesch et al. 2007; Yoshida et al. 2006; Ouchi et al. 2004; Steidel et al. 1999), following $M_*(z) = -21.02 + 0.36(z-3.8)$ (Bouwens et al. 2008), and previous studies suggested a similar trend to $z \sim 7$ (e.g., Bouwens et al. 2008; Oesch et al. 2009a; Ouchi et al. 2009). From our simulations we estimate that 31 ± 8 objects should be detected in our small area survey, assuming no evolution of the LF since $z \sim 6$ (error bars include uncertainties in the LF parameters). The cosmic variance is expected to add 35%–40% (Trenti & Stiavelli 2008). While the expected number of sources is much larger than the 16 observed, the difference is not yet statistically robust. Clearly, the combination of our survey with wider area data will provide much stronger constraints on the changes from $z \sim 6$ to $z \sim 7$ in the future.

To better quantify the evolution of the LBG population, we show the stepwise LF based on our data in Figure 4. Absolute magnitudes are computed assuming all candidates to lie at $z \sim 6.8$ and the effective volume is estimated as $V_{\rm eff}(m) = \int_0^\infty dz \frac{dV}{dz} S(z,m) C(m)$.

Due to the small area of the present data we are not able to fit all parameters of the Schechter function from our data set alone. We therefore include the points from wide area Subaru searches

for $z \sim 7$ galaxies by Ouchi et al. (2009) in order to constrain the bright end of the LF. The fitting is done as in Oesch et al. (2009a) maximizing the Poissonian likelihood for the observed number of sources in each magnitude bin.

The value of ϕ_* of the UV LF has been found to be remarkably constant with redshift, and we fix its value to $\phi_* = 1.4 \times 10^{-3}$ Mpc^{-3} mag^{-1} as measured at $z \sim 6$ (Bouwens et al. 2007). This results in $M_* = -19.91 \pm 0.09$ and $\alpha = -1.77 \pm 0.20$, which gives a first constraint on the faint-end slope at $z \sim 7$. This Schechter function is shown in Figure 4 as a black solid line.

The data are consistent with a faint-end slope that is largely unchanged over the 2.5 Gyr from $z \sim 7$ to $z \sim 2$ with a value of $\alpha \sim -1.7$ (e.g., Reddy et al. 2009; Bouwens et al. 2007; Oesch et al. 2007), and the measured value of M_* is in very good agreement with the extrapolation of Bouwens et al. (2008). Note also that, within the error bars, the LF function parameters are consistent with the ones derived by Ouchi et al. (2009).

4. SUMMARY AND CONCLUSIONS

The first observations with the WFC3/IR camera have demonstrated the amazing improvement over previous NIR instruments. Nevertheless, they have confirmed our prior NICMOS detections at $z \sim 7$. In the first epoch data of the HUDF09, which comprises only about one third of the final data set, we have identified a robust sample of 16 $z \sim 7$ galaxy candidates down to flux limits as low as 29 mag. With NICMOS about 100 orbits were needed per $z \sim 7$ galaxy candidate found (Bouwens et al. 2009a); WFC3 is ~40 times more efficient and requires only 2.4 orbits per candidate (for fields with existing deep optical data). This remarkable ability to detect high redshift galaxies extends to $z \gtrsim 8$ (see Bouwens et al. 2009b)

Most of the $z \sim 7$ candidates appear very compact with an average observed half-light radius of ~0.″16 (from SExtractor apertures) indicating that the typical size of a starburst galaxy at $z \sim 7$ is of the order of $\lesssim$1 kpc (for a more extensive analysis of galaxy sizes, see Oesch et al. 2009b).

Due to the depth of our observations we can put a first constraint on the faint end of the LF at $z \sim 7$ of $\alpha = -1.77 \pm 0.20$. This is consistent with no evolution over the whole time span from $z \sim 7$ until $z \sim 2$ and such a steep faint-end slope has strong implications for reionization, providing support to a scenario in which low-luminosity galaxies provide the bulk of the flux for ionizing the universe (see also Oesch et al. 2009a; Kistler et al. 2009). The combined surface brightness of our sources is $\mu_J \simeq 26.1$ mag arcmin^{-2} which is brighter than the minimum required for reionization at ~7 for Population II stars $\mu_{\rm min} \simeq 27.2$ (Stiavelli et al. 2004a, 2004b). The factor ~3 difference suggests that even considering an escape fraction $\ll$1, these galaxies still contribute significantly to reionization.

The full HUDF09 data set, complemented with planned wide area surveys, will allow another leap forward in the measurement of the $z \sim 7$ LF in the near future. The *HST* is again enabling a revolutionary advance in our understanding of the build-up of galaxies in the universe.

We especially thank all those at NASA, STScI, and throughout the community who have worked so diligently to make *Hubble* the remarkable observatory that it is today. The servicing missions, like the recent SM4, have rejuvenated *HST* and made it an extraordinarily productive scientific facility time and time again, and we greatly appreciate the support of policy makers, and all those in the flight and servicing programs who contributed to the repeated successes of the *HST* servicing missions. P.O. acknowledges support from the Swiss National Foundation (SNF). This work has been supported by NASA grant NAG5-7697 and NASA grant HST-GO-11563.01. This research has benefitted from the SpeX Prism Spectral Libraries, maintained by Adam Burgasser at http://www.browndwarfs.org/spexprism.

Facilities: *HST* (ACS/NICMOS/WFC3)

REFERENCES

Beckwith, S. V. W., et al. 2006, AJ, 132, 1729
Bertin, E., & Arnouts, S. 1996, A&A, 117, 393
Bouwens, R. J., & Illingworth, G. D. 2006, Nature, 443, 189
Bouwens, R. J., et al. 2004a, ApJ, 611, 1
Bouwens, R. J., et al. 2004b, ApJ, 616, L79
Bouwens, R. J., et al. 2007, ApJ, 670, 928
Bouwens, R. J., et al. 2008, ApJ, 686, 230
Bouwens, R. J., et al. 2009a, ApJ, 690, 1764
Bouwens, R. J., et al. 2009b, ApJ, submitted (arXiv:0909.1803)
Bouwens, R. J., et al. 2009c, ApJ, 705, 936
Bouwens, R. J., et al. 2009d, ApJ, in press (arXiv:0910.0001)
Bradley, L. D., et al. 2008, ApJ, 678, 647
Bruzual, G., & Charlot, S. 2003, MNRAS, 344, 1000
Burgasser, A. J., et al. 2004, AJ, 127, 2856
Bunker, A. J., et al. 2009, MNRAS, in press (arXiv:0909.2255)
Burrows, A., et al. 2006, ApJ, 640, 1063
Calzetti, D., et al. 2000, ApJ, 533, 682
Castellano, M., et al. 2009, A&A, in press (arXiv:0909.2853)
Coe, D., et al. 2006, AJ, 132, 926
Coleman, G. D., et al. 1980, ApJS, 43, 393
Ferguson, H. C., et al. 2004, ApJ, 600, 107
Giavalisco, M., et al. 2004, ApJ, 600, L103
Kistler, M. D., et al. 2009, ApJ, 705, L104
Koekemoer, A., et al. 2002, in HST Calib. Workshop, ed. S. Arribas, A. M. Koekemoer, & B. Whitmore (Baltimore: STScI), 337
Labbé, I., et al. 2006, ApJ, 649, L67
McLure, R. J., et al. 2009a, MNRAS, 395, 2196
McLure, R. J., et al. 2009b, MNRAS, in press (arXiv:0909.2437)
Oesch, P. A., et al. 2007, ApJ, 671, 1212
Oesch, P. A., et al. 2009a, ApJ, 690, 1350
Oesch, P. A., et al. 2009b, ApJ, in press (arXiv:0909.5183)
Oke, J. B., & Gunn, J. E. 1983, ApJ, 266, 713
Ouchi, M., et al. 2004, ApJ, 611, 660
Ouchi, M., et al. 2009, ApJ, 706, 1136
Pinfield, D. J., et al. 2008, MNRAS, 390, 304
Reddy, N. A., et al. 2009, ApJ, 692, 778
Richard, J., et al. 2008, ApJ, 685, 705
Stanway, E., et al. 2005, MNRAS, 359, 1184
Steidel, C., et al. 1996, ApJ, 462, L17
Steidel, C., et al. 1999, ApJ, 519, 1
Stiavelli, M., et al. 2004a, ApJ, 610, L1
Stiavelli, M., et al. 2004b, ApJ, 600, 508
Thompson, R. I., et al. 2005, AJ, 130, 1
Trenti, M., & Stiavelli, M. 2008, ApJ, 676, 767
Yan, H., & Windhorst, R. A. 2004, ApJ, 612, L93
Yoshida, M., et al. 2006, ApJ, 653, 988
Zheng, W., et al. 2009, ApJ, 697, 1907